Applied Catalysis B: Environmental 256 (2019) 117889

Contents lists available at ScienceDirect

Applied Catalysis B: Environmental

journal homepage: www.elsevier.com/locate/apcatb

Selective catalytic decarboxylation of biomass-derived carboxylic acids to bio-based methacrylic acid over hexaaluminate catalysts

Ashish Bohre*, Brigita Hočevar, Miha Grilc, Blaž Likozar*

Department of Catalysis and Chemical Reaction Engineering, National Institute of Chemistry, Hajdrihova 19, 1000 Ljubljana, Slovenia

ARTICLE INFO

Keywords:
Biomass-derived itaconic acid
Bio-based methacrylic acid
Resource valorization process
Catalytic decarboxylation reaction
Heterogeneous catalyst material

ABSTRACT

Methacrylic acid (MAA) is a polymer molecular constituent in related plastics industry, presently produced from supplied fossil-based resources. This scientific paper reports an environmentally-benign catalytic process for the production of MAA via the decarboxylation of carboxylic groups. Various hexaaluminate catalysts were synthetized examined and tested to achieve the maximum amount yield of MAA from biomass derived carboxylic acids. Active phases on catalyst surfaces were characterized with numerous microscopic, spectroscopic and chemi-/physi-sorption techniques. Among hexaaluminate catalysts, the highest selectivity towards MAA (50%) was accomplished over barium hexa-aluminate at relatively mild reaction conditions (3 h, 250 °C and 20 bar). In addition, the catalyst could be reused four times without the loss of activity. A plausible pathway mechanism was also hypothesized. The high catalytic activity of BHA catalyst compared to the other tested catalysts believed to be associated with its peculiar layered structure, surface defect sites, moderate basicity and high surface area. The newly developed catalyst and corresponding process avoid the use of expensive noble or transition metals and corrosive alkalis. Overall, the development of catalysis presents a step forward in the synthesis of a sustainable structural constituent.

1. Introduction

Modern society depends heavily on fossil resources for the production of polymers. It is difficult to imagine the world without plastics, or synthetic organic polymers [1]. The global production of polymers has exceeded 8300 million metric tons (Mt) to date, that consumes ~7% fossil fuels worldwide [2,3]. The finite nature of petrochemical sources and aggravated change of environmental conditions have driven an initiative both in academia and industry toward generating sustainable polymers derived from renewable biomass feedstock [4]. Incorporation of renewable polymers has achieved great progress in the bio-based polymer market. However, inferior performance and high production cost compared to petroleum-derived polymers should be addressed to meet the current market demands.

Methacrylic acid (MAA) and methyl methacrylate (MMA) are specialty monomers applied in diverse industries including electronics, paints and coating, optical fibers, adhesives and sealants [5]. The vast varieties of applications are increasing the demand of MAA and MMA worldwide (4.8 million tons by 2020), which is increasing the price by 10% annually [6]. The majority of MAA is being produced from petrochemical sources through different processes such as acetone cyanohydrin (ACH) process (Lucite), New ACH process (Mitsubishi gas chemicals), C_2 approach (BASF), Alpha route (Lucite), Isobutene process (Mitsubishi Rayon) etc. [7,8]. Besides the use of fossil sources, low atom economy, poor product selectivity, the toxicity of the substrates are other drawbacks associated with industrial processes [9]. Demand-supply gap for MAA and unsustainable utilization of fossil feedstock have driven the academia and industries to develop new processes with lower carbon footprint.

Several bio-based routes to MMA and MAA were reported in the literature in which at least one raw material is produced from bio sources [10,11,12]. For instance, acetone and ethanol are main raw materials for ACH process that can be produced by the fermentation of plant crops [10]. Similarly, raw materials like ethylene and isobutene for C_2 and C_4 approaches can be produced by the fermentation of plant biomass [13,14].

Decarboxylation is an important step, widely applied in chemical industry to obtain valuable products such as butanone, C_9-ketone, C17 hydrocarbon, anisol, benzyl cyanide and 2-methylbutyronitrile via the reaction of levulinic acid, 6-amyl-a-pyrone, stearic acid, ortho-anisic acid, isoleucine and phenyl alanine, respectively [15,16,17,18]. One such process involved the decarboxylation of itaconic acid (IA) and citric acid to MAA. IA is a carbohydrate- derived aliphatic dicarboxylic acid considered as the cleanest alternative to petroleum-based acrylic

* Corresponding authors.
E-mail addresses: ashish.bohre@ki.si (A. Bohre), blaz.likozar@ki.si (B. Likozar).

https://doi.org/10.1016/j.apcatb.2019.117889
Received 19 February 2019; Received in revised form 14 June 2019; Accepted 19 June 2019
Available online 20 June 2019
0926-3373/

acid [19]. Citric acid is a much more widely available renewable precursor derived from the fermentation of carbohydrates and are found abundantly in juices of citrus fruits [20]. The first report on catalytic decarboxylation of biomass-derived substrates such as IA to MAA was published in 1994 by Magnus Carlsson and his coworkers. Excellent yield (72%) of MAA was obtained but the reaction temperature was relatively high (350 °C) [21]. In 2014, Le Nôtre et al. reported high selectivity in the aqueous decarboxylation of IA to MAA using a 5 wt% Pt/Al_2O_3 catalyst and NaOH as a co-catalyst [22]. However, utilization of noble metal makes this process expensive and on the other hand, the alkaline base is corrosive and neutralization of the waste water stream is expensive. Later, M. Pirmoradi and James R. Kastner reported a liquid base free approach for the synthesis of MAA from biomass-derived IA, citric acid and 2-hydroxyisobutyric acid in 2016 [23]. High yields of 76% were achieved at 275 °C using 2-hydroxyisobutyric acid and subcritical water. However, in case of IA only 23% MAA was achieved under the optimum reaction conditions over hydrotalcite catalyst. The other potentially viable methods to produce MMA and MAA including aldol condensation of ethyl propionate with formaldehyde, oxidative esterification of methacrolein, oxidative dehydrogenation of methyl isobutyrate etc. are also reported in the literature [24,25,26]. In addition to the existing catalytic routes, biotechnological routes to convert renewable carbohydrates into MAA have been envisaged by using non-naturally occurring microbial organism [27].

A better solid base catalyst or support for a base catalyst than hydrotalcite is hexaaluminates, widely used for high temperature applications such as natural gas combustion, carbon dioxide reforming of methane, partial oxidation of hydrocarbon and nitrous oxide decomposition [28]. These materials exhibit remarkable thermal stability and sintering resistance, which make them suitable candidates for high temperature applications [29,30]. The high catalytic activity and thermal stability of hexaaluminate materials are associated with their unique layered structure of alternately stacked spinel blocks separated by mirror planes [31,32].

The specific surface area of hexaaluminate materials are low ($20\ m^2\ g^{-1}$) due to the high crystallization temperature (> 1200 °C) accompanied by grain growth. The catalytic activity of hexaaluminates can be remarkably enhanced by increasing the surface area. Many preparation strategies have been developed to improve the surface area, such as coupling of a sol–gel process in reverse microemulsions, and solid-state reaction followed by two steps of ball milling have been developed [33]. However, it is impossible to produce hexaaluminates on a large scale by the above routes due to the high energy-consumption, constraints of scalability, economic, and safety issues. Therefore, a new facile method to enhance the surface area is highly desired.

Inspired by the pioneer work of Santiago et al. herein we have prepared high surface area hexaaluminate catalysts through carbon templating route [34]. To the best of our knowledge, this is the first report on utilization of hexaaluminate catalysts for decarboxylation reaction. The work described in this paper has several advantages over the previously published works [9,20,21,22]. Most notably, this work brings improvements in the use of heterogeneous catalyst by avoiding corrosive base additives and precious metals like Pt and Ru. The as-prepared hexaaluminate catalysts showed high activity for the decarboxylation of biomass derived feedstocks for the synthesis of MAA.

2. Experimental

2.1. Chemicals

IA, citric acid, aconitic acid, MAA, mesaconic acid, crotonic acid, citraconic acid, 2-hydroxyisobutaric acid, pyruvic acid, acetic acid, acetone, hexane, toluene, tetrahydrofuran, ethanol, methanol, and acetonitrile were purchased from Sigma Aldrich. Calcium nitrate, aluminium nitrate nonahydrate, magnesium nitrate, barium nitrate, ammonium carbonate, phosphoric acid, sodium hydroxide, hydrochloric acid and carbon black were purchased from Alfa Aesar. All the chemicals were highly pure (> 99%) and used as received.

2.2. Catalysts preparation

Barium hexaaluminate (BHA) catalyst was prepared by following the literature procedure [35]. Appropriate amounts of $Ba(NO_3)_2$ and $Al(NO_3)_3{\cdot}9H_2O$ were dissolved in deionized water at 60 °C. Subsequently, 40 g of carbon black as a hard template was added to reduce the agglomeration of BHA particles during crystallization at high temperature, and the mixture was stirred overnight to get precursor slurry. Next, $(NH_4)_2CO_3$ was dissolved in deionized water and stirred for 1 h at 60 °C. Subsequently, the slurry of BHA was poured into an $(NH_4)_2CO_3$ solution and the mixture was vigorously stirred for 4 h to obtain a gel. The obtained gel was filtered, washed with deionized water and dried in vacuum at 110 °C overnight. The obtained powder was calcined in Ar at 1250 °C for 5 h, followed by calcination at 900 °C in air for 12 h to completely remove the carbon, leading to a BHA catalyst with high surface area. BHA-15, BHA-20 and BHA-25 catalyst with 15 mol %, 20 mol % and 25 mol % loading of barium, calcium hexaaluminate (CHA), lanthanum hexaaluminate (LHA), and magnesium hexaaluminate (MHA) were also prepared by the same preparation method as described above.

2.3. Catalyst characterization

The crystalline phases of hexaaluminate catalysts were identified by powder X-ray diffraction (XRD) and recorded on PW3040/60 X'Pert PRO MPD diffractometer which was operated at 45 kV and 40 mA with CuK_α radiation source ($\lambda = 0.154056$ nm) at room temperature by a step size of 0.02° in 2θ range from 10° to 80°. The identification of crystalline phases and diffraction peaks was referred to the JCPDS database. Average crystallite sizes of the supports and catalysts were calculated from the full width at half-maximum (FWHM) of the most intense peak by applying Scherrer's equation.

The surface area and pore volume of the samples were determined from N_2 physisorption isotherms. The measurements were conducted at $T = -196$ °C using a Micromeritics ASAP 2020 M P/C apparatus. The specific surface area was determined using the Brunauer–Emmett–Teller (BET) method. Prior to characterization, the samples were degassed under N_2 flow for 4 h at 200 °C. Barrett − Joyner − Halenda (BJH) was used for the calculation of the pore size distribution. It was applied using the modified Kelvin equation. It relates the amount of adsorbate removed from the pores of the materials as the relative pressure (P/P_0) is decreased from a greater to smaller value with respect to the pore size. Cumulative pore volume was calculated from the amount of N_2 adsorbed at a relative pressure P/P_0 of 0.99. They were reported alongside average pore size and BET specific surface area data.

Carbon dioxide temperature programmed desorption (CO_2-TPD) measurements were performed by using Micromeritics AutoChem II 2920 apparatus on 250 mg of catalyst samples. The catalysts were pretreated at 350 °C under the helium purge for 60 min. The temperature was consequently decreased to 80 °C. 9.8 mol % CO_2 in He was passed over the catalysts at the flow rate of 30 ml min^{-1} for 60 min. The excess gas was removed by purging with helium for 30 min. The temperature was after that gradually (10 K min^{-1}) raised to 900 °C under the helium flow and amount of desorbed CO_2 was recorded. The total reactive gas desorption were measured. To convert the peak area data to volume data, the analyser was calibrated with gas mixtures of known composition. For the calculation of the number of basic sites, it was assumed that only one molecule of CO_2 can adsorb on a single site.

Particle size and morphology were investigated using high-resolution transmission electron microscopy (HRTEM). Micrographs were obtained by using a JEOL JEM-3010 instrument operated at 300 kV, equipped with a LaB_6 filament coupled with energy-dispersive X-ray

probe (EDS).

2.4. Catalytic activity measurement

The activity measurements were carried out in a high-pressure batch reactor (system of 6 parallel batch reactors, each of 250 mL, Amar Equipment Pvt. Ltd., India) equipped with a thermocouple, pressure gauge, rupture disk, gas and liquid sampling line. In a typical experiment, biomass-derived carboxylic acid was dissolved in deionized water. The solution was loaded into the autoclave reactor with a catalyst and sealed. The reactor was pressurized with N_2 to 10 bar and vented three times to remove any residual oxygen. Finally, the pressure of the reactor was raised to the desired pressure with N_2, stirred by the Rushton turbine (600 min^{-1}). The recorded reaction time started when the temperature reached the desired set-point (typically heating up to 250 °C was achieved in 40 min). Once the reaction time expired, the reactor was cooled down to the room temperature (20 °C). After collecting final gas and liquid sample, pressure from the headspace of the reactor was released. Selectivity (S_a) was calculated according to the following formula:

$$Sa = (Ya/C) \times 100$$

in which Y_a is the yield of compound a and C is the conversion of carboxylic acids in the reaction mixture.

The crude reaction mixture was analysed by ultra-high performance liquid chromatography - UHPLC (Thermo-Fisher Scientific UltiMate 3000) equipped with Acclaim Organic Acid LC Columns (5.0 μm; 4 × 25 mm) heated to 45 °C and DAD detector (λ = 210 nm). Gas phase analysis in the headspace was performed by using 490 Micro GC (Agilent) operating at a sample line temperature of 30 °C with helium and argon as a carrier gas. The gaseous products were separated by CP-Molsieve and PoraPolt U columns and detected by using TCD.

After purification of MAA from the crude mixture by distillation and solvent extraction process as described in the literature [22]. ^1H and ^{13}C spectral analysis was performed in $CDCl_3$ medium on a JEOL JNM ECX-400 P 400 MHz instrument and data were processed using JEOL Delta NMR software (Figure S1 and Figure S2, ESI†). Chemical shifts were expressed in ppm (δ-scale). Splitting patterns are described as singlet (s), doublet (d), triplet (t), quartet (q) and multiplet (m).

MAA: ^1H NMR ($CDCl_3$, 400 MHz): δ = 1.93 (dd, 3 H), 5.66 (m, 1 H), 6.23 (m. 1 H), 12.20 ppm (br s, 1 H); ^{13}C NMR ($CDCl_3$): δ = 17.76, 127.80, 135.75, 173.25 ppm.

3. Results and discussion

3.1. Structural and physicochemical characterization

The crystal structure type of the hexaaluminate materials depend upon the atomic radius and charge density of the large cations in the mirror planes. For instance, barium hexaaluminate (BHA) has assigned the β-alumina structure, whereas lanthanum hexaaluminate (LHA), calcium hexaaluminate (CHA) and magnesium hexaaluminate (MHA) belongs to the magnetoplumbite structure [36,37]. When higher valence ions like Ba^{2+} replace the sodium, considerable numbers of BR sites (Beevers–Ross sites) are empty, creating a population of vacancies and surface defects in BHA catalyst [38]. The detailed defect mechanism of barium hexaaluminate has been reviewed in the literature [39,40].

Powder XRD patterns of the hexaaluminate catalysts are shown in Fig. 1. For the BHA catalyst, the peaks at 19°, 27°, 34°, and 38°, indicating a relatively pure BHA crystalline phase without any intermediate and $BaCO_3$ phase formation [41]. In contrast to BHA catalyst, the XRD pattern of CHA (CA_6) exhibited the mixed phases of $CaO{\cdot}Al_2O_3$ (CA), $CaO{\cdot}2Al_2O_3$ (CA_2), and $CaO{\cdot}6Al_2O_3$ (CA_6), respectively [42]. The presence of different calcium aluminate phases were due to the low calcination temperature, as the high temperature required (> 1500 °C)

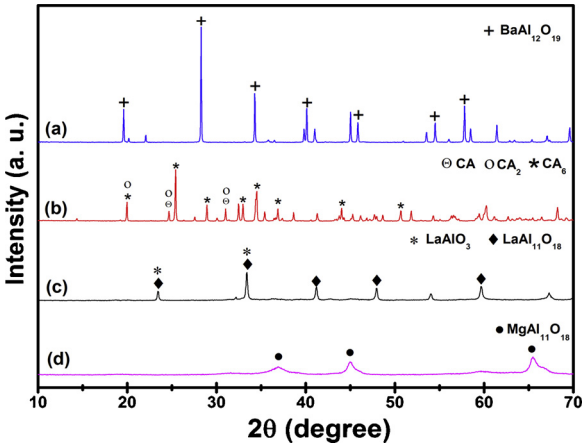

Fig. 1. Diffraction patterns of the (a) BHA, (b) CHA, (c) LHA, and (d) MHA catalysts.

to prepare pure phase of CHA catalyst [43,44]. However, no residual CaO or other CaO-containing phases were detected by the XRD. The diffraction pattern of LHA showed the formation of LHA ($LaAl_{11}O_{18}$) as the major phase while, lanthanum monoaluminate (LMA, $LaAlO_3$) and alumina appear as secondary phase [45]. This is in accordance with the study of Cinibulk et al. that reveals the two stages formation of LHA [46]. In first stage LMA is formed easily at lower temperature (< 800 °C) while complete conversion to LHA requires long reaction time (94 h) and high temperature (1650 °C). For the MHA catalyst, a low crystallinity phase was observed compared to other hexaaluminate catalysts. In addition to this, the presence of amorphous MgO and alumina were also observed [47].

The textural characteristics of hexaaluminate catalysts are summarize in Table 1. Notably, the surface area of hexaaluminate catalysts were much higher than the previous reports [48,49], demonstrating that adopting carbon black (CB) as template can effectively prevent the agglomeration of particles during the high temperature calcination process, and thus increase the surface area [35]. The difference in the surface area among different hexaaluminate catalysts could be attributed to the base metal present in the hexaaluminate structure. The crystallite sizes determined by diffraction patterns of hexaaluminate catalysts were all in the range of 15–70 nm.

Fig. 2 shows nitrogen adsorption-desorption isotherms for the hexaaluminate catalysts. All the catalysts showed a similar pattern in adsorption-desorption isotherms and displayed an approximate type IV isotherm (IUPAC) with a hysteretic loop at relative pressures p/p° range of 0.70-0.89 indicated the mesoporous character of the catalysts. The desorption isotherms support data obtained from nitrogen physisorption that the catalysts have a uniform pore size distribution (Figure S3). It was observed that the distribution of pore size and isotherm remained constant over the range of metals present on the surface of hexaaluminate catalysts indicating that the metallic species did not disturb the pore structure but was incorporated into the framework of hexaaluminate. Interestingly, the incorporation of alkali metal increase the

Table 1
Particulate properties of hexaaluminate catalysts.

Catalyst	Surface area [$m^2\ g^{-1}$]	Pore volume [$cm^3\ g^{-1}$]	Mean crystallite size[a] [nm]	Average Pore size [nm]
BHA	95.8	0.46	18	18.4
CHA	8.2	0.04	31	33.4
LHA	25.0	0.32	28	39.2
MHA	105	0.48	68	21.5

[a] calculated from XRD using Scherrer equation.

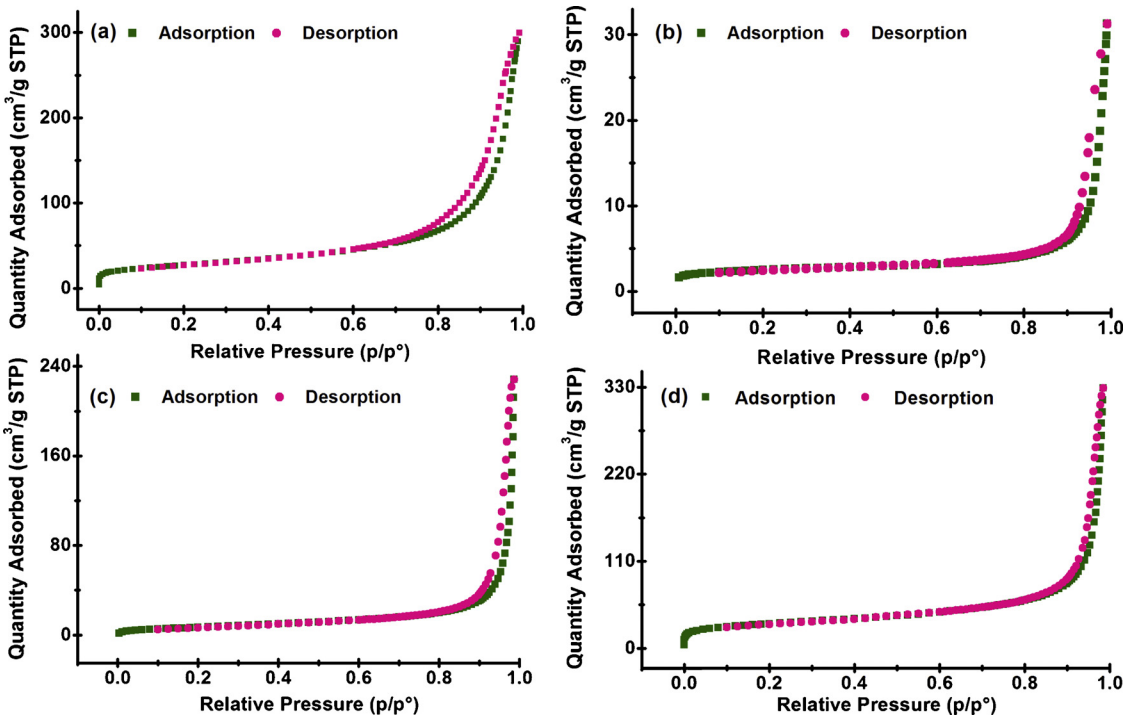

Fig. 2. Nitrogen adsorption-desorption isotherms of (a) BHA, (b) CHA, (c) LHA, and (d) MHA catalysts.

pore width of the catalysts due to the bond length of Al-O that is greater than of M–O (M = Ca^{2+}, La^{2+}, Mg^{2+}, Ba^{2+}).

The CO_2-TPD curves of hexaaluminate catalysts are presented in Fig. 3. It is apparent from CO_2-TPD profiles that all prepared catalysts showed at least two CO_2 desorption peaks: 1 st peak centered at lower temperature (around 50–200 °C) and 2nd peak centered at relatively higher temperature (around 200–400 °C). These desorption peaks are assigned to the low and medium strength basic sites which could be

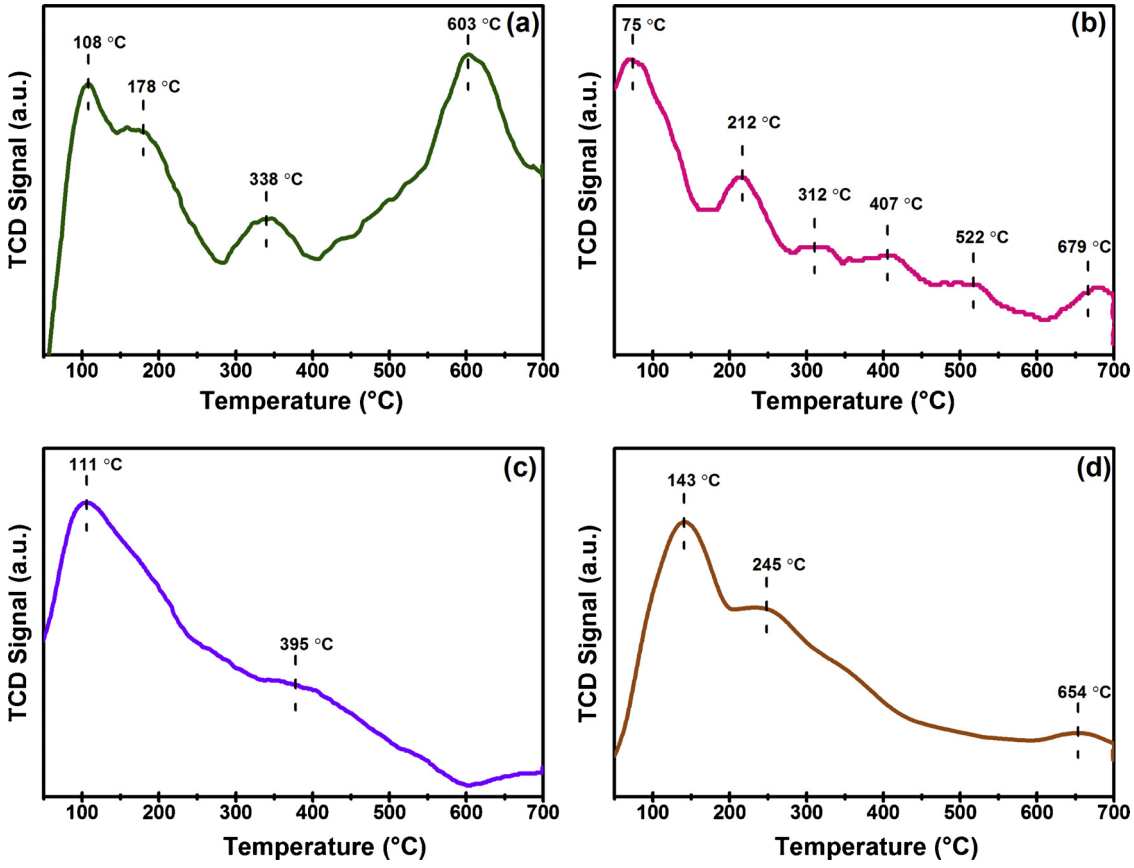

Fig. 3. CO_2-TPD profiles of (a) BHA, (b) CHA, (c) LHA and (d) MHA catalysts.

Table 2
Distribution of basic sites on hexaaluminate catalysts.

Catalyst	Number of basic sites [μmol g^{-1}]			
	Weak[a]	Moderate[b]	Strong[c]	Total
BHA	0.5	1.0	1.5	3.0
CHA	1.2	1.6	1.3	4.1
LHA	1.0	0.7	0.0	1.7
MHA	1.2	0.8	0.5	2.5

[a] $T < 250$ °C, [b] $T = 250–500$ °C and [c] $T > 500$ °C.

associated to surface HO^-, M^{2+}-$O^{2-}$and Al^{3+}-O^{2-} Lewis acid-base pairs, respectively. Moreover, for BHA and CHA catalysts one broad desorption peak was observed at around 500–650 °C which is attributed to strong basic sites related to the low-coordination surface O^{2-} anion [28]. The quantitative distribution of basic sites on the surface of hexaaluminate catalysts were calculated from a deconvolution of CO_2-TPD profiles by using AutoChem 2920 software and were summarized in Table 2 [50,51]. As expected, CHA and LHA were observed to be the most and the least basic catalysts, respectively. In general, alumina consists of weak basic sites, which are modified by the presence of alkaline base metals in hexaaluminate catalysts. In multicomponent mixed oxides, a simpler situation is represented by the case, in which only two types of cations are present. When the two have similar oxidation states and electronegativity, the global acidic-alkaline characteristics are often dominated by those of one of the two components [52,53]. Thus, in the present case, the basic character of the catalysts is strongly pronounced by the presence of alkaline metal when compared to alumina. These results are in sufficient accordance with as reported by other researchers for hexaaluminate catalysts [54].

Fig. 4 shows the TEM images of hexaaluminate catalysts. Two distinctive morphologies can be clearly seen in the TEM images of the catalysts, one with big crystallites and the other one with small agglomerates. The big crystallites seem to grow in the form and shape of platelets and the small agglomerates show features in the form of needle. Interestingly, in case of MHA catalyst, clear hexagonal platelets of different nanometric sizes (50–200 nm) can be seen. Crystalline nature of the BHA, CHA and LHA catalysts can be ascertained from the spots observed in the select area electron diffraction (SAED) patterns. In good agreement with the XRD pattern, amorphous morphology was observed for MHA catalyst. TEM-EDX mapping analysis showed the uniform distribution of each element (Figure S4-S7, ESI†). Interestingly, the segregation of Ba^{2+} ions on the mirror planes and grain boundaries were observed in the high resolution TEM image of BHA catalyst (Fig. 5). This might me due to the presence of crystal disorders and defects on the surface of BHA catalyst [39a].

3.2. Catalytic performance

It was reported in the literature that basicity of the catalyst plays a vital role for the formation of MAA [21]. To proof our concept we have selected barium, calcium, magnesium and lanthanum hexaaluminates with different basic site densities. We have evaluated the catalytic activity of hexaaluminate catalysts by varying the reaction conditions such as reaction time, temperature, pressure and pH of the reaction mixture. The purpose for designing these experiments was to optimise the reaction conditions and maximise the yield of MAA. We have first investigated the effect of reaction temperature at constant pressure on the selectivity of MAA without the addition of catalyst (Figure S8, ESI†). It is noteworthy that the yield of MAA was increased with temperature and the highest yield of MAA (29%) was obtained at 250 °C. This is due to the dissociation of water into hydronium and hydroxide ions under our experimental conditions that acts as a catalyst for the

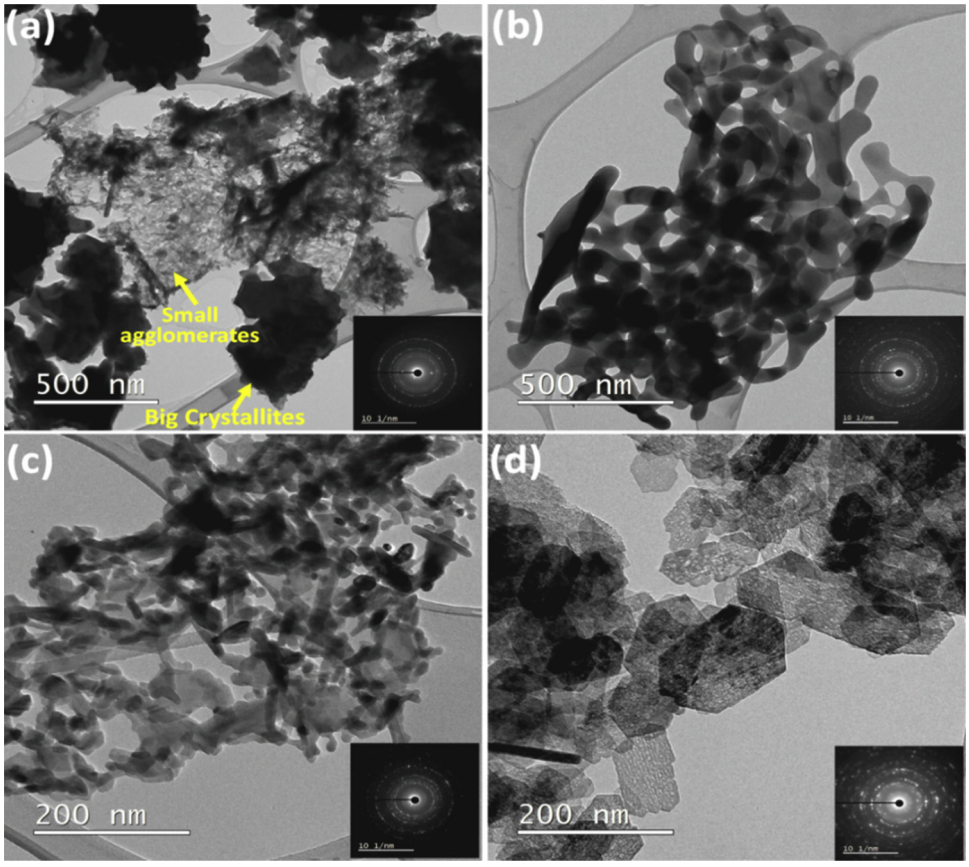

Fig. 4. Transmission electron micrographs select area electron diffraction (SAED) (inset) of (a) BHA, (b) CHA, (c) LHA and (d) MHA catalysts.

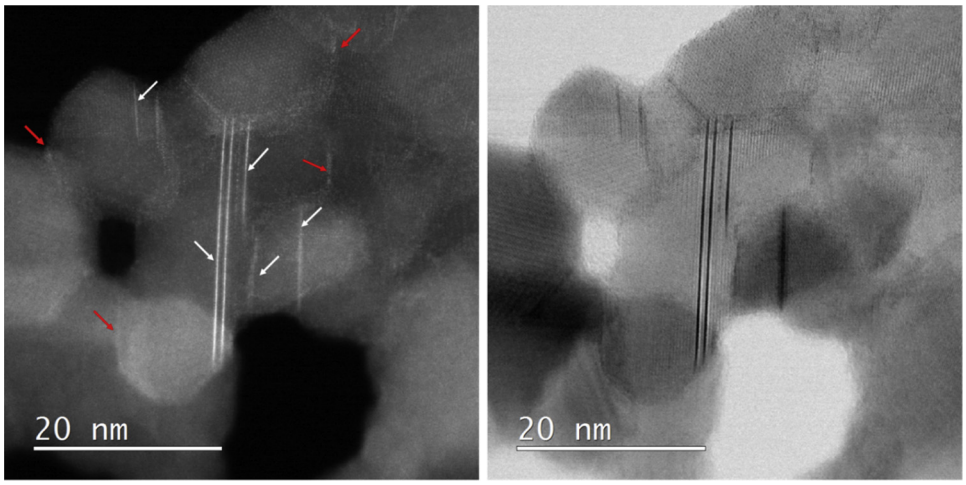

Fig. 5. HRTEM images of BHA catalyst showing the segregation of barium ion on complete single plane on some of the crystallites (marked white arrows) and on the grain boundaries (marked with red arrows) (For interpretation of the references to colour in this figure legend, the reader is referred to the web version of this article).

Table 3
Effect of reaction temperature on decarboxylation of itaconic acid to MAA with hexaaluminate catalysts.

Entry [a]	Catalysts	*T* [°C]	Conversion [%]	Selectivity [mol%]			
				MAA	Isomers[b]	2-HIBA	AA	Others[c]
1	CHA	200	62	11	9	9	–	9
2	CHA	250	100	38	–	16	11	35
3	CHA	275	100	22	–	10	26	42
4	MHA	200	68	11	8	–	8	41
5	MHA	250	100	40	–	–	38	22
6	MHA	275	100	23	–	–	41	36
7	LHA	200	65	10	7	9	23	16
8	LHA	250	100	12	–	8	62	18
9	LHA	275	100	7	–	3	63	27
10	BHA	200	59	37	8	11	6	38
11	BHA	250	100	50	–	18	3	29
12	BHA	275	100	27	–	8	30	38

[a] Reaction conditions : IA (2 g), solvent (water, 150 mL), time (3 h), pressure (20 bar), catalyst (1 g), [b] Isomers = mesaconic acid + citraconic acid, [c] Others = pyruvic acid, crotonic acid, acetone, propene and carbon dioxide. Values were determined by HPLC and micro-GC. IA is itaconic acid, MAA is methacrylic acid, AA is acetic acid and 2-HIBA is 2-hydroxyisobutyric acid.

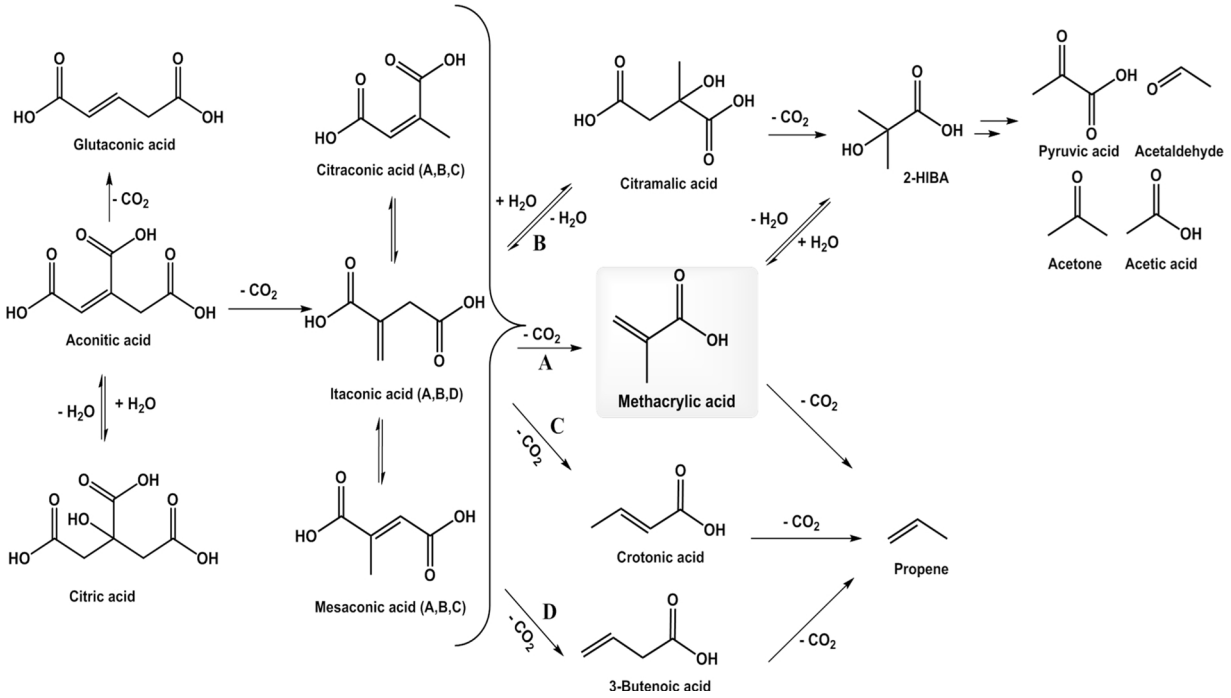

Scheme 1. Reaction network for the decarboxylation of citric acid, aconitic acid and itaconic acid.

decarboxylation of IA [55]. In the second set of experiments, we have tested the catalytic activity of hexaaluminate catalysts by varying the reaction temperature (Table 3). Based on the previous literature data, we have studied reaction temperatures in the range 200–275 °C [21,22]. In our reaction system it was observed that the MAA yield and IA conversion were increased when the reaction temperature was raised from 200 to 250 °C. At the reaction temperature of 250 °C, hexaaluminate catalysts showed high catalytic activity compared with those experiments performed below and above this temperature. At low temperatures the conversion of IA is incomplete and more isomers were present in the reaction mixture. It appears that degradation had already occurred from the observation of fragmentation products. Isomerization was anticipated because extensive isomerization of double bond location and geometry [22], whereas the presence of 2-hydroxyisobutyric acid (2-HIBA) confirmed that degradation started through the hydration and decarboxylation of IA (Scheme 1, pathway B). High temperature (> 250 °C) resulted in complete IA conversion but lower MAA selectivity. This was attributed to the high acidity of the reaction medium at higher set temperature [39b]. High acidity of the reaction mixture affects the acid adsorbed on catalyst surface; it would be because of the possibility of removing the adsorbed acid from the surface and replacing it by water [21].

The catalytic activity was further investigated by tuning the pressure of the reaction in the second set of experiments, while the temperature was kept constant (Table S1, ESI†). As expected, catalytic reactions performed without any added external N_2 pressure over hexaaluminate catalysts led to poor selectivity of MAA and accelerated the isomers formation. Furthermore when the pressure was increased (> 30 bar) under these conditions, the selectivity of MAA decreased and the formation of side products predominated indicating that a higher pressure is not favorable in this case. Under high N_2 pressure the formation of excess amount of acetic acid (Table S1) increased the pH of the reaction mixture and could promotes the parasitic reactions as confirmed by the pH variation experiments. Notably, under these reaction conditions a 4 bar increase of the internal pressure was observed probably caused by the formation of gaseous by-products due to the subsequent decarboxylation and hydration steps [9]. To prevent the polymerization of MAA during the reaction, we have performed one experiment under the optimized reaction conditions with the addition of 4-methoxyphenol polymer inhibitor (200 ppm) over BHA catalyst. Unfortunately, it did not improve the yield of MAA.

It was confirmed from the CO_2-TPD results shown in Table 2 and Fig. 3 that the basicity of the catalyst affects the MAA yield. For instance, LHA and CHA catalysts with low and high basicity yielded 12% and 22% MAA under optimized reaction conditions, respectively. In contrast, BHA and MHA catalyst exhibited moderate basicity and produce 40% and 50% MAA, respectively. These observations are in accordance with results obtained from the pH variation experiments (Fig. 6). Previous reports noted that effective catalysis for the decarboxylation of MAA depends on the basicity of the catalyst [23]. The increased in basicity of the catalyst promotes the formation of by-products and decreased the selectivity to the target product. The catalyst with moderate basicity favours the decarboxylation reaction of IA.

To further test the effect of basicity on the yield of MAA, we have prepared three BHA catalysts with different barium loading. As observed from the Table S2 and Figure S9-S11, ESI †, the yield of MAA decreased with increased barium loading (> 10 Mol %) due to the low dispersion of barium ion in the matrix of hexaaluminate and high basicity of the catalysts. On the other hand, incorporation of 10 Mol % barium metal ions in Al^{3+} positions of the spinel blocks enables to introduce active catalytic sites in the structure [30].

It can be seen from the Scheme 1, that most of the side products were formed by the addition of water molecule. To prevent the formation of side products we have performed the decarboxylation under the presence of different solvents (Table 4). We began our investigation with nonpolar solvents under the optimized reaction conditions.

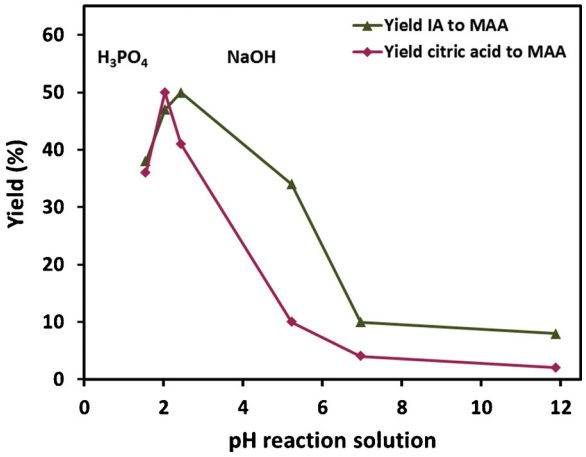

Fig. 6. Decarboxylation of IA and citric acid over BHA catalyst at different pH values. Reaction condition is shown in Table 3, entry 11.

Table 4
Solvent effect on decarboxylation of itaconic acid to MAA over BHA catalyst.

Entry[a]	Solvent	Polarity[63]	Conversion [%]	Yield [%]
1	Hexane	0.06	negligible	–
2	Toluene	2.40	28	8
3	THF	4.20	62	18
4	EtOH	4.30	67	23
5	CH_3CN	6.20	75	31
6	MeOH	6.60	79	39
7	H_2O	10.2	100	50

[a] Reaction conditions: Itaconic acid (2 g), solvent (150 mL), catalyst (1 g), initial pressure (20 bar), *t* (3 h), *T* (250 °C).

Nonpolar solvents such as hexane and toluene showed relatively poor conversion and yield of IA (Table 4, entry 1–2). Changing the solvents to more polar solvents such as acetonitrile and methanol gradually increased the yield and conversion, and reached to the maximum with water, highlighting its greener and sustainable nature. Water is a necessary component for the decarboxylation of IA to MAA as it mitigates formation of anhydrides and enhanced the yield of MAA [56]. It was reported in the literature that the addition of water accelerate the decarboxylation step for carboxylic acids through the hydration of the carboxyl group [57].

3.3. Conversion of citric acid and aconitic acid to MAA

Encouraged by the successful application in the conversion of IA, the scope of the BHA catalyst was explored with widely available biomass-derived chemicals such as aconitic acid and citric acid, whereas the latter is much more available renewable resource. It is produced commercially either by submerged fermentation or surface fermentation employing various carbohydrate sources [58]. Interestingly, IA can also be produced via a high yield fermentation process using citric acid. Citric acid decarboxylate directly to IA without going first into aconitic acid. It can proceed by protonation of the −OH group and its departure to the same carbocation with the positive centre in the beta position to one of the carboxylic groups. MAA was produced by the decarboxylation of IA, whereas vinyl group on beta position relative to the carboxylic group assists forming a positive charge of beta-carbon, which is responsible for accelerated decarboxylation [57]. The reaction with citric acid was initially performed under the previously optimized reaction condition (Table 3, entry 11). Surprisingly high yield of 50% MAA with complete conversion of citric acid was observed (Table 5, entry 1). To further improve the reaction efficiency, a set of factors including the concentration of citric acid, temperature, pressure and

Table 5
Effect of reaction conditions on decarboxylation of citric acid to MAA with barium hexaaluminate catalyst.

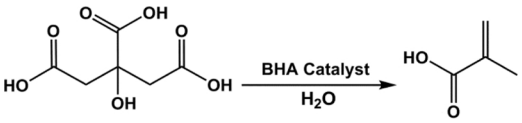

Entry[a]	Citric acid [M]	*P* [bar]	*T* [°C]	Conversion [%]	Selectivity [mol %]			
					MAA	AA 2-HIBA		Others[b]
1	0.10	20	250	100	50	6	16	28
2	0.15	20	250	100	45	15	17	23
3	0.10	20	275	100	39	8	6	47
4	0.10	30	250	100	47	7	22	24
5	0.10	40	250	100	47	9	19	25
6	0.10[c]	20	250	100	46	7	17	30

[a] Reaction conditions : Citric acid, solvent (water), time (3 h), catalyst (1 g), [b] Others = pyruvic acid, crotonic acid, acetone, propene and carbon dioxide, [c] time (4 h). Values were determined by HPLC and micro-GC. MAA is methacrylic acid, AA is acetic acid and 2-HIBA is 2-hydroxyisobutyric acid.

reaction time was screened. However, the variations of reaction parameters have not improved the yield of MAA.

MAA was produced by the decarboxylation of IA, whereas vinyl group on beta position relative to the carboxylic group assists forming a positive charge of beta-carbon, which is responsible for accelerated decarboxylation [58]. Eventual double bond migration or isomerisation in IA forms citraconic or mesaconic acid, where protonation of their double bond can lead to the formation of either crotonic or methacrylic acid. On the other hand protonation of vinyl group in IA (positive charge on beta-carbon) could only be selectively converted to MAA via decarboxylation (A) (Scheme 1), while decarboxylation to 3-Butenoic acid is less likely, as there is no moiety to stabilize a positive charge on the beta-position.

After successful testing of BHA catalyst for the production of MAA from IA and citric acid, the scope of the catalyst was further extended for decarboxylation of aconitic acid. Aconitic acid is obtained by the acid catalysed dehydration of citric acid. Aconitic acid occurres naturally in sugarcane, beetroot and sorghum. The raw sugarcane juice contains around 1–2 g L^{-1} of aconitc acid and sugarcane molasses contain amounts of aconitic acid ranging from 0.9% to 5.5% (on a dry solids basis). Moreover, fermentation routes to aconitic acid have also been reported in the literature [59]. With the optimized conditions in hand, the BHA catalysed decarboxylation of aconitic acid was investigated. Interestingly, we have achieved similar yield of MAA (51%) with complete conversion of aconitic acid. Aconitic acid is obviously being decarboxylated to IA with nearly 100% selectivity in the first step, as it could theoretically also form glutaconic acid (grey in Scheme 1) that cannot be further converted to MAA. Despite we cannot conclude from our experimental results whether citric acid was converted into IA directly or via aconitic acid intermediate, however we demonstrated that a selectivity of the overall conversion of citric acid to IA is nearly 100%, therefore the contribution of parasitic reactions can be considered negligible. Further conversion of IA into MAA is far less selective due to the parallel reactions of double-bond migration and further cis-trans isomerisation and hydration of an alkene group. Double bond migration reactions were reported to have much lower activation energies (21–45 kJ mol^{-1}) compared to decarboxylation (134–140 kJ mol^{-1}) on $NiMo/Al_2O_3$, therefore the temperature increase accelerates the decarboxylation rates much faster than isomerisation rates, which would results in higher selectivity towards decarboxylation [60]. However, results in Table 3 show that temperature above 250 °C lowered the yield of MAA, as it was further decarboxylated to propene or hydrated to other products. Based on the results, we can conclude that the residence time is still to be optimized, as well as the selection of the reactor type, as continuous fixed-bed reactor might help reducing the residence time and improving MAA selectivity. Based on the state of the art, the selectivity of BHA catalyst is still surprisingly high and is believed to be associated with its peculiar layered structure, surface defect sites, moderate basicity and high surface area.

3.4. Effects of pH: IA conversion and MAA yield

With such impressive results in hand, lastly, we have investigated the effect of pH on the decarboxylation reaction of IA and citric acid to MAA over BHA catalyst (Fig. 6). The pH was varied by the addition of H_3PO_4 or NaOH; the natural pH of the starting solution (concentration, solvent) at room temperature was 2.5. The addition of H_3PO_4 strongly reduced the decarboxylation of IA to MAA; yielded 38% of MAA with 85% conversion at pH 1.5. When the pH was adjusted to 2.0, the yield of MAA was increased to 47% at 96% conversion. Interestingly, when one control experiment was performed at pH 2.0 under the similar reaction conditions without the addition of BHA catalyst, the yield of MAA was only 32%. Low pH favours the hydrolytic degradation of IA by the addition of water molecules to double bonds that result in acetic acid, acetone, and other side products formation and reduces the yield of MAA [21]. We have detected 2-hydroxyisobutyric acid, acetone, pyruvic acid and acetic acid in all the crude reaction mixture confirmed that in acidic environment pathway B was predominated (Scheme 1). Similar to the acidic pH, alkaline pH also had a critical influence on the selectivity towards MAA. The yield of MAA was 34% at pH 5.2 that significantly decrease to 10% at the neutral pH of 7.0 and reached to 8% under the strongly basic environment (pH = 11.5). This suggests that hydroxide ions participate in the parasitic reaction pathway by the hydrolysis of IA [61]. Similar to our observations with IA, the addition of an acid or a base led to poorer results when citric acid was tested over BHA catalyst at different pH values (Fig. 6). Simple lowering of the pH (to assist the double bond protonation), does not increase the rate of decarboxylation, therefore BHA must play an important role with its ability to bind carboxylic group to a metal centre for an exchange of the carboxylic proton. Deprotonated carboxylic acid then readily protonate a double bond and result in C—C bond cleavage by decarboxylation.

3.5. Recyclability of the BHA catalyst

In view of the good results obtained with the BHA catalyst, we decided to explore the catalyst stability by exploring their recyclability. For reusability, after completion of each run, the reaction mixture was allowed to reach room temperature, and the solid catalyst was separated by centrifugation, washed with water, dried, and reused in the subsequent run. As shown in Fig. 7, that the activity of BHA catalyst

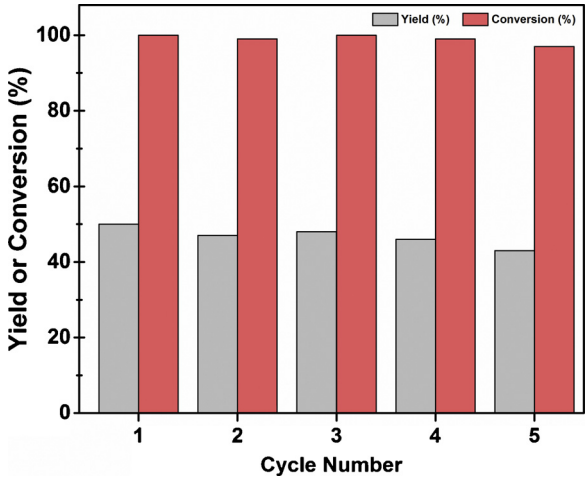

Fig. 7. Recycling tests of BHA catalyst for the decarboxylation of IA to MAA. Reaction condition is shown in Table 3, entry 11.

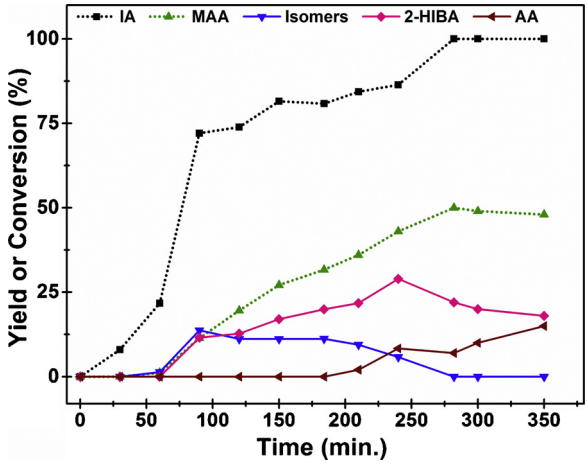

Fig. 8. Time dependent results of IA decarboxylation over the BHA catalyst. Reaction condition is shown in Table 3, entry 11.

reduced by 7% fifth cycle. This could also be partly attributed to the loss of the catalyst mass (7%) during the recovery also account for such variation in catalytic activity. The high thermal stability of BHA catalyst are associated with their peculiar layered structure, consisting of alternatively stacked spinel blocks of $[Al_{11}O_{16}]^+$ and mirror planes in which large barium cations are located [62].

3.6. Time profile of decarboxylation with BHA catalyst

To study the reaction mechanism, a reaction kinetic was conducted. As can be seen in Fig. 8, in the first 60 min of the reaction, much isomer were formed and there was a small quantity of MAA in the product. As prolonging reaction time, the isomers gradually disappeared accompanied by an increase in the yield of MAA, thereafter, it remains constant (50%) up to 350 min. Thus, the kinetics of MAA formation is rapid in first 180 min followed by a slow reaction. The possible reaction pathway for the decarboxylation of IA to MAA is shown in Scheme 2. First, IA was isomerized to mesaconic acid and citraconic acid. In the second step, IA was adsorbed on the catalyst surface. The presence of active sites on the surface of BHA catalyst abstracts the proton from IA to form itaconate monoanion that has a higher rate of decarboxylation. The generated carbonium ion further decarboxylates to MAA by leaving the β-carboxyl group [61]. Subsequently, the second decarboxylation of MAA produces propene (Scheme 1, reaction **A**). It was observed that the formation of side products started from the beginning by following parallel pathways. Under hydrothermal conditions in reaction **B**, any of the three IA isomers can add the water across the double bond forming, citramalic acid. However, we have not detected citramalic acid in the reaction mixture. Citramalic acid is not stable and further decarboxylate to 2-hydroxyisobutyric acid (2-HIBA). Finally, the radical fragmentation of 2-HIBA leads to the formation of degradation products [58]. In reaction **C,** the itaconic isomers decarboxylated to crotonic acid. The rate of decarboxylation of itaconic isomers to crotonic acid is slow, proven by the presence of traces of crotonic acid (< 1%) in reaction mixtures [21]. Lastly, the second decarboxylation of itaconic isomers produces propene.

4. Conclusions

In summary, various hexaaluminate catalysts have been successfully applied for the decarboxylation of biomass-derived carboxylic acids to MAA. In general, the BHA catalyst gave the highest yield (50%) compared to other catalysts. We have optimized the reaction conditions by changing the reaction temperature, pressure, and solvent system to achieve the maximum yield of MAA. Temperature and pressure variation experiments reveal that high temperature (> 250 °C) and pressure (> 20 bar) promotes the side products formation. Solvent variation experiments over BHA catalyst showed that the polarity of the solvent plays a vital role in the decarboxylation reaction of IA. The improved conversion of IA and MAA yield were achieved with polar solvents such as methanol and water. The most active BHA catalyst also exhibited superior activity for the decarboxylation of biomass-derived citric acid and aconitic acid to MAA (Yield ~50%). The results of the reusability test also showed that BHA catalyst had a good stability and had a good catalytic activity even at the end of the fourth cycle. The high catalytic activity of BHA catalyst compared to the other tested catalysts is associated with its peculiar layered structure, moderate basicity, surface defect sites and high surface area.

Acknowledgements

The authors gratefully acknowledge the financial support of the Slovenian Research Agency (ARRS) through the Program P2 – 0152. The work was partially carried out within the RDI project Cel. Cycle: «Potential of biomass for the development of advanced materials and bio-based products, co-financed by the Republic of Slovenia, Ministry of Education, Science and Sport and European Union under the European Regional Development Fund, 2016–2020.

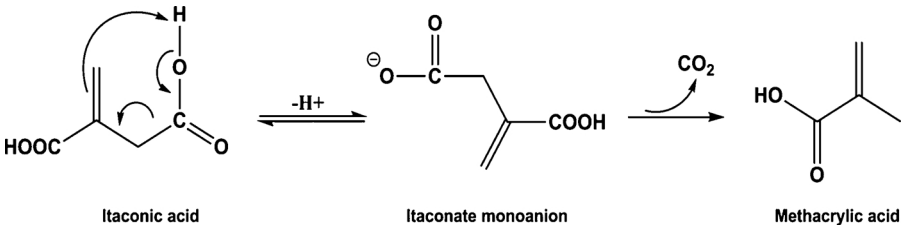

Scheme 2. Proposed reaction route for the decarboxylation of itaconic acid to methacrylic acid.

Appendix A. Supplementary data

Supplementary material related to this article can be found, in the online version, at doi:https://doi.org/10.1016/j.apcatb.2019.117889.

References

[1] R. Geyer, J.R. Jambeck, K.L. Law, Production, use, and fate of all plastics ever made, Sci. Adv. 3 (7) (2017) 1–5.
[2] K. Yao, C. Tang, Controlled polymerization of next-generation renewable monomers and beyond, Macromolecules 46 (2013) 1689–1712.
[3] M. Rabnawaz, I. Wyman, R. Auras, S. Cheng, A roadmap towards green packaging: the current status and future outlook for polyesters in the packaging industry, Green Chem. 19 (2017) 4737–4753.
[4] Z. Sun, Bl. Fridrich, A. de Santi, S. Elangovan, K. Barta, Bright side of lignin depolymerization: toward new platform chemicals, Chem. Rev. 118 (2) (2018) 614–674.
[5] J. Verduyckt, D.E. De Vos, Controlled defunctionalisation of biobased organic acids, Chem. Commun. 53 (2017) 5682–5693.
[6] M.J.D. Mahboub, J.L. Dubois, F. Cavani, M. Rostamizadeh, G.S. Patience, Catalysis for the synthesis of methacrylic acid and methyl methacrylate, Chem. Soc. Rev. 47 (2018) 7703–7738.
[7] Y.L. Cao, L. Wang, B.H. Xu, S.J. Zhang, The Chitin/Keggin-type heteropolyacid hybrid microspheres as catalyst for oxidation of methacrolein to methacrylic acid, Chem. Eng. J. 334 (2018) 1657–1667.
[8] M.J. Darabi Mahboub, J.L. Dubois, F. Cavani, M. Rostamizadeh, G.S. Patience, Catalysis for the synthesis of methacrylic acid and methyl methacrylate, Chem. Soc. Rev. 47 (2018) 7703–7738.
[9] J.C. Lansing, R.E. Murray, B.R. Moser, Biobased Methacrylic acid via selective catalytic decarboxylation of itaconic acid, ACS Sustain. Chem. Eng. 5 (2017) 3132–3140.
[10] J.L. Dubois, J.F. Crolzy, L. Campora, C. Croizy, P. Croizy, Biomass-derived Methyl Methacrylate and Corresponding Manufacturing Method, Uses and Polymers, (2011) US20110318515A1.
[11] J.L. Dubois, Method for Manufacturing a Biomass-derived Methyl Methacrylate, (2011) US20110287991A1.
[12] D.W. Johnson, G.R. Eastham, M. Poliakoff, T.A. Huddle, A Process for the Production of Methacrylic Acid and Its Derivatives and Polymers Produced Therefrom, (2011) EP2643283B1.
[13] A. Mohsenzadeh, A. Zamani, M.J. Taherzadeh, Bioethylene Production from ethanol: a review and techno-economical evaluation, ChemBioEng. Rev. 4 (2017) 75–91.
[14] B.N. van Leeuwen, A.M. van der Wulp, I. Duijnstee, A.J. van Maris, A.J. Straathof, Fermentative production of isobutene, Appl. Microbiol. Biotechnol. 93 (2012) 1377–1387.
[15] W. Zhang, M. Ma, M. Huijbers, G.A. Filonenko, E.A. Pidko, M. van Schie, S. de Boer, B.O. Burek, J. Bloh, W.J. van Berkel, Hydrocarbon synthesis via photoenzymatic decarboxylation of carboxylic acids, J. Am. Chem. Soc. 141 (7) (2019) 3116–3120.
[16] G.J.S. Dawes, E.L. Scott, J. Le Notre, J.P. Sanders, J.H. Bitter, Deoxygenation of biobased molecules by decarboxylation and decarbonylation–a review on the role of heterogeneous, homogeneous and bio-catalysis, Green Chem. 17 (2015) 3231–3250.
[17] T. Patra, D. Maiti, Decarboxylation as the key step in C-C bond-forming reactions, Chem. Eur. J. 23 (2017) 7382–7401.
[18] M.I. Alam, S. Gupta, A. Bohre, E. Ahmad, T.S. Khan, B. Saha, M.A. Haider, Development of 6-amyl-α-pyrone as a potential biomass-derived platform molecule, Green Chem. 18 (2016) 6431–6435.
[19] R. Bafana, R. Pandey, New approaches for itaconic acid production: bottlenecks and possible remedies, Crit. Rev. Biotechnol. 38 (2018) 68–82.
[20] B. Yu, X. Zhang, W. Sun, X. Xi, N. Zhao, Z. Huang, Z. Ying, L. Liu, D. Liu, H. Niu, Continuous citric acid production in repeated-fed batch fermentation by Aspergillus niger immobilized on a new porous foam, J. Biotechnol. 276 (2018) 1–9.
[21] M. Carlsson, C. Habenicht, L.C. Kam, M.J.J. Antal, N. Bian, R.J. Cunningham, M.J. Jones, Study of the sequential conversion of citric to itaconic to methacrylic acid in near-critical and supercritical water, Ind. Eng. Chem. Res. 33 (1994) 1989–1996.
[22] J. Le Nôtre, S.C.Witte-van Dijk, J. van Haveren, E.L. Scott, J.P. Sanders, Synthesis of bio-based methacrylic acid by decarboxylation of itaconic acid and citric acid catalyzed by solid transition-metal catalysts, ChemSusChem 7 (2014) 2712–2720.
[23] M. Pirmoradi, J.R. Kastner, Synthesis of methacrylic acid by catalytic decarboxylation and dehydration of carboxylic acids using a solid base and subcritical water, ACS Sustain. Chem. Eng. 5 (2016) 1517–1527.
[24] J. Gao, G. Fan, L. Yang, X. Cao, P. Zhang, F. Li, Oxidative esterification of methacrolein to methyl methacrylate over gold nanoparticles on hydroxyapatite, ChemCatChem 9 (2017) 1230–1241.
[25] A. Harilal, V.D. Dasireddy, H.B. Friedrich, An oxidative route for the production of methyl methacrylate: a study over iron phosphate catalysts, Catal. Lett. 146 (2016) 1169–1181.
[26] B. Li, R. Yan, L. Wang, Y. Diao, Z. Li, S. Zhang, Synthesis of methyl methacrylate by aldol condensation of methyl propionate with formaldehyde over acid–base bifunctional catalysts, Catal. Lett. 143 (2013) 829–838.
[27] K. Nagai, New developments in the production of methyl methacrylate, Appl. Catal. A Gen. 221 (2001) 367–377.
[28] M. Tian, X. Wang, T. Zhang, Hexaaluminates: a review of the structure, synthesis and catalytic performance, Catal. Sci. Technol. 6 (2016) 1984–2004.
[29] L.-c. Yan, L.T. Thompson, Synthesis and characterization of aerogel-derived cation-substituted barium hexaaluminates, Appl. Catal. A Gen. 171 (1998) 219–228.
[30] M. Santiago, J. Pérez-Ramírez, Decomposition of N_2O over hexaaluminate catalysts, Environ. Sci. Technol. 41 (2007) 1704–1709.
[31] N. Iyi, S. Takekawa, S. Kimura, Crystal chemistry of hexaaluminates: β-alumina and magnetoplumbite structures, J. Solid State Chem. 83 (1989) 8–19.
[32] X. Li, K. Zhu, J. Pang, M. Tian, J. Liu, A.I. Rykov, M. Zheng, X. Wang, X. Zhu, Y. Huang, Unique role of Mossbauer spectroscopy in assessing structural features of heterogeneous catalysts, Appl Catal B. Environ. 224 (2018) 518–532.
[33] F. Huang, X. Wang, A. Wang, J. Xu, T. Zhang, A two-step synthesis of Fe-substituted hexaaluminates with enhanced surface area and activity in methane catalytic combustion, Catal. Sci. Technol. 6 (2016) 4962–4969.
[34] M. Santiago, J.C. Groen, J. Perez-Ramirez, Carbon-templated hexaaluminates with enhanced surface area and catalytic performance, J. Catal. 257 (2008) 152–162.
[35] J. Gao, C. Jia, M. Zhang, F. Gu, G. Xu, Z. Zhong, F. Su, Template preparation of high-surface-area barium hexaaluminate as nickel catalyst support for improved CO methanation, RSC Adv. 3 (2013) 18156–18163.
[37] P.K. Sahu, B. Kulkarni, R. Khomane, S. Pardhy, U. Phalgune, P. Rajmohanan, R. Pasricha, Barium hexaaluminate nanowhiskers synthesized by novel sol–gel process in reverse micellar media, Chem. Commun. (2003) 1876–1877.
[38] N. Iyi, Z. Inoue, S. Takekawa, S. Kimura, The crystal structure of barium hexaaluminate phase I (barium β-alumina), J. Solid State Chem. 52 (1984) 66–72.
[39] (a) J.G. Park, A. Cormack, Crystal/defect structures and phase stability in Ba hexaaluminates, J. Solid State Chem. 121 (1996) 278–290;
(b) K. Chandler, F. Deng, A.K. Dillow, C.L. Liotta, C.A. Eckert, Alkylation reactions in near-critical water in the absence of acid catalysts, Ind. Eng. Chem. Res. 36 (1997) 5175–5179.
[40] J. Wang, On the charge compensation mechanism in β-alumina, J. Chem. Phys. 73 (1980) 5786–5795.
[41] J.C. Debsikdar, Synthesis and characterization of gel-derived barium hexa-aluminate, J. Mater. Sci. 24 (1989) 3565–3572.
[42] S. Iftekhar, J. Grins, G. Svensson, J. Loof, T. Jarmar, G.A. Botton, C.M. Andrei, H. Engqvist, Phase formation of $CaAl_2O_4$ from $CaCO_3$-Al_2O_3 powder mixtures, J. Eur. Ceram. Soc. 28 (2008) 747–756.
[43] V.K. Singh, K.K. Sharma, Low-temperature synthesis of calcium hexa-aluminate, J. Am. Ceram. Soc. 85 (2002) 769–772.
[44] D. Asmi, I. Low, Physical and mechanical characteristics of in-situ alumina/calcium hexaluminate composites, J. Mater. Sci. Lett. 17 (1998) 1735–1738.
[45] Z. Negahdari, M. Willert-Porada, F. Scherm, Thermal properties of homogenous lanthanum hexaaluminate/alumina composite ceramics, J. Eur. Ceram. Soc. 30 (2010) 3103–3109.
[46] M.K. Cinibulk, Synthesis and characterization of sol-gel derived lanthanum hexaaluminate powders and films, J. Mater. Res. 10 (1995) 71–76.
[47] K. Ovanesyan, A. Kuzanyan, G. Badalyan, A. Yeganyan, R. Sargsyan, V. Kuzanyan, A. Petrosyan, V. Stathopoulos, Preparation and investigation of rare earth magnesium hexaaluminate solid solutions, Contemp. Phys. 49 (2014) 220–227.
[48] M.F. Zwinkels, S. Druesne, P.G. Menon, E. Björnbom, S.G. Järås, Thermal stability of complex oxide combustion catalyst supports, Ind. Eng. Chem. Res. 37 (1998) 391–397.
[49] A. Sánchez-Herencia, R. Moreno, C. Baudın, Fracture behaviour of alumina–calcium hexaluminate composites obtained by colloidal processing, J. Eur. Ceram. Soc. 20 (2000) 2575–2583.
[50] Š. Hajduk, V.D. Dasireddy, B. Likozar, G. Dražić, Z.C. Orel, COx-free hydrogen production via decomposition of ammonia over Cu–Zn-based heterogeneous catalysts and their activity/stability, Appl Catal B. Environ. 211 (2017) 57–67.
[51] M. Akri, O. Achak, P. Granger, S. Wang, C. Batiot-Dupeyrat, T. Chafik, Autothermal reforming of model purified biogas using an extruded honeycomb monolith: A new catalyst based on nickel incorporated illite clay promoted with MgO, J. Clean. Prod. 171 (2018) 377–389.
[52] M. Jabłońska, R. Palkovits, Copper based catalysts for the selective ammonia oxidation into nitrogen and water vapour-recent trends and open challenges, Appl. Catal. B 181 (2016) 332–351.
[53] Z. Yuan, L. Wang, J. Wang, S. Xia, P. Chen, Z. Hou, X. Zheng, Hydrogenolysis of glycerol over homogenously dispersed copper on solid base catalysts, Appl. Catal. B 101 (2011) 431–440.
[54] M.V. Bukhtiyarova, A.S. Ivanova, L.M. Plyasova, G.S. Litvak, A.A. Budneva, E.A. Paukshtis, Structure and acid-base properties of hexaaluminates, React. Kinet. Catal. Lett. 93 (2008) 375–387.
[55] P.E. Savage, Organic chemical reactions in supercritical water, Chem. Rev. 99 (1999) 603–622.
[56] R.D. Gandour, Structural requirements for intramolecular proton transfers, Tetrahedron Lett. 15 (1974) 295–298.
[57] (a) A.V. Ignatchenko, J.P. McSally, M.D. Bishop, J. Zweigle, Ab initio study of the mechanism of carboxylic acids cross-ketonization on monoclinic zirconia via condensation to beta-keto acids followed by decarboxylation, Mol. Catal. 441 (2017) 35–62;
(b) R. Kluger, Catalyzing decarboxylation by taming carbon dioxide, Pure Appl. Chem. 87 (4) (2015) 353–360.
[58] (a) E. Alben, O. Erkmen, Production of citric acid from a new substrate, undersized semolina, by Aspergillus niger, Food Technol. Biotechnol. 42 (2004) 19–22;
(b) J. Verduyckt, D.E. De Vos, Highly selective one-step dehydration, decarboxylation and hydrogenation of citric acid to methylsuccinic acid, Chem. Sci. 8 (2017) 2616–2620.
[59] K. Kobayashi, J. Maruebi, K. Kirimura, Bioproduction of trans-aconitic acid from citric acid by whole-cell reaction of Escherichia coli heterologously expressing the

aconitate isomerase gene from Pseudomonas sp. WU-0701, ChemistrySelect 1 (2016) 1467–1471.

[60] (a) B. Hočevar, M. Grilc, M. Huš, B. Likozar, Mechanism, ab initio calculations and microkinetics of straight-chain alcohol, ether, ester, aldehyde and carboxylic acid hydrodeoxygenation over Ni-Mo catalyst, Chem. Eng. J. 359 (2019) 1339–1351;
(b) B. Hočevar, M. Grilc, M. Huš, B. Likozar, Mechanism, ab initio calculations and microkinetics of hydrogenation, hydrodeoxygenation, double bond migration and cis–trans isomerisation during hydrotreatment of C6 secondary alcohol species and ketones, Appl. Catal. B 218 (2017) 147–162;
(c) M. Grilc, B. Likozar, Levulinic acid hydrodeoxygenation, decarboxylation and oligmerization over NiMo/Al_2O_3 catalyst to bio-based value-added chemicals: modelling of mass transfer, thermodynamics and micro-kinetics, Chem. Eng. J. 330 (2017) 383–397.

[61] J. Li, T.B. Brill, Spectroscopy of hydrothermal solutions 18: pH-dependent kinetics of itaconic acid reactions in real time, J. Phys. Chem. A 105 (2001) 10839–10845.

[62] Y. Zhang, X. Wang, Y. Zhu, X. Liu, T. Zhang, Thermal Evolution crystal structure and Fe crystallographic sites in $LaFe_xAl_{12-x}O_{19}$ hexaaluminates, J. Phys. Chem. C 118 (2014) 10792–10804.

[63] C. Reichardt, T. Welton, Solvents and Solvent Effects in Organic Chemistry, John Wiley & Sons, 2011.